Research Journal of Recent Sciences _____ ISSN 2277-2502
Vol. **2(9),** 5-10, September **(2013)** *Res.J.Recent Sci.*

Analytical solution for wave diffraction around cylinder

Fatimah Noor Harun
Dept. of Mathematics, Faculty of Sci. & Tech., Universiti Malaysia Terengganu 21030 Kuala Terengganu, Terengganu Darul Iman, MALAYSIA

Available online at: www.isca.in
Received 29th January 2013, revised 14th April 2013, accepted 7th July 2013

Abstract

Waves are one of the energy resources that intensively studying nowadays. The awareness about climate changes, global warming etc makes many researchers interested in developing the new source of the renewable energy by using the ocean waves. The energy from waves is become popular because it is the natural energy and it does not extinct like other sources of energy such as oil. One of the technologies to extract the energy from ocean waves that is becoming popular among the researchers nowadays is oscillating water column (OWC). In this paper, the mild-slope equation is further extended to be applied to the OWC problem. The mild slope equation is a powerful tool to study the phenomenon of combined refraction-diffraction of ocean waves over a mild topography. Therefore, in this paper, we will present the analytical solution for the long waves propagating over a circular hump located at the bottom of an ocean with a hollow circular cylinder floating on the top of the free surface. Then, an example is given to compare our new analytic solution in a special case of the two-layer fluid model, i.e $h_2 = 0$ with the solution obtained by Mac Camy and Fuchs. To further verify our solution, we have also compared our solution when the hump height, d is small enough with the flat bottom. Then, by using the new solution, we then discuss the effects of the hump dimensions and the hollow cylinder structures on the wave diffraction. Finally, the main findings in this chapter will be briefly summarized at the end of this paper.

Keywords: analytical solution, mild-slope equation, renewable wave energy.

Introduction

In recent years, there has been a great deal of interest in renewable energy resources with regards to combating climate changes. One of the renewable energy resources comes from ocean waves. Many researchers have been impressed by the force and energy extracted from the ocean waves. Renewable analysts believe that the global power potential represented by waves that hit all coastlines worldwide is estimated to provide up to 1 TW (1 terawatt=10^{12} watt). Therefore, ocean waves represent an enormous source of renewable energy as it is believed that the market potential for energy from the waves is in a very high demand if the technology to extract the energy from waves is successfully developed. A variety of technologies have been proposed to capture the energy from the waves. These technologies can be installed either in onshore or offshore locations. One of the technologies to extract the energy from ocean waves that is becoming popular among the researchers nowadays is oscillating water column (OWC)[1].

The OWC consists of a partially submerged concrete or steel structure that has an opening to the sea below the waterline. It encloses a column of air above a column of water. As waves enter the air column, they cause the water column to rise and fall. This alternately compresses and depressurizes the air column. As the wave retreats, the air is drawn back through the turbine as a result of the reduced air pressure on the ocean side of the turbine. Figure 1 is one of the examples of an OWC prototype installed by Oceanlinx Limited Australia at Port Kembla, NSW, Australia. This device has successfully converted ocean wave energy into electricity in a number of tests being conducted since it was installed.

Figure-1
An OWC prototype locate at Port Kembla, NSW, Australia

Early theories for OWC are introduced by Garret[2], who solved the first order diffraction problem for a suspended cylinder in ocean of a finite depth. Since then, various mathematical approaches of problems relating to OWC devices have been discussed in the literature over the years. For examples, many authors had presented their work related to a simple two-dimensional OWC models, such as Evans[3,4], Smith[5], and Sarmento and Falcе*a*o[6]. Recently, Falcе*a*o and Rodrigues[7] and Falcе*a*o[8] had developed a stochastic model to evaluate the

average performance of an OWC energy device equipped with Wells turbine.

More recently, Martin-rivas and Mei[9] have carried out a theoretical study of a single OWC being installed at the tip of a breakwater, with vertical circular cylinder open in all direction. In the same year, they also presented the linearized theory of an OWC installed on a straight coast with the vertical cylinder half embedded in the cliff and open on the seaside[10].

In this paper, we construct an analytic solution for long waves propagating over a circular hump located at the bottom of a single-layer ocean but with the hollow cylinder floating at the top of the free surface. Then, in section 3, an example is given to compare our new analytic solution in a special case of the two-layer fluid model, i.e $h_2 = 0$ with the solution obtain by Mac Camy and Fuchs[11]. Using the new solution, we then discuss the effects of the hump dimensions and the hollow cylinder structures on the wave refraction. Finally, the main findings in this paper are briefly summarized in section 4.

Methodology

In this section, we presented the derivation of the mild-slope equation in a two-layer fluid model with free surface on the top by removing the rigid lid approximation that have been discussed by Zhu and Harun[12] . For the OWC problem, we will treat our case as for a single layer problem. Then, we will used the results that we have derived for the mild-slope equation in a two-layer fluid to solve an OWC problem. The reason that we have solved our problem using the two-layer model is, we need to satisfy all the boundary conditions that exist in this case. By using the two-layer fluid model, it is much easier to determine the boundary condition in both layers. Hence, in this section, first, the two-layer fluid model is presented. Then, we use the result to derive an analytic solution for long waves that are propagating over a circular hump and also over a flat bottom with a hollow cylinder located at the free surface.

The two-layer fluid model: Considering a two-layer system depicted in Figure 2, under a Cartesian Coordinate system in which x and y denote a pair of orthogonal horizontal coordinates and z denotes the vertical coordinate measured positively upwards from the free surface. By assuming that the two fluids are immiscible, the flow within each layer is irrotational, the free surface and the interfacial waves are of small amplitude relative to their wavelength, the velocity potential Φ(x, y, z, t) can be written as

$$\Phi(x,y,z,t) = \begin{cases} \Phi_1(x,y,z,t), & -h_1 \le z \le 0, \\ \Phi_2(x,y,z,t), & -h \le z \le -h_1. \end{cases} \quad (1)$$

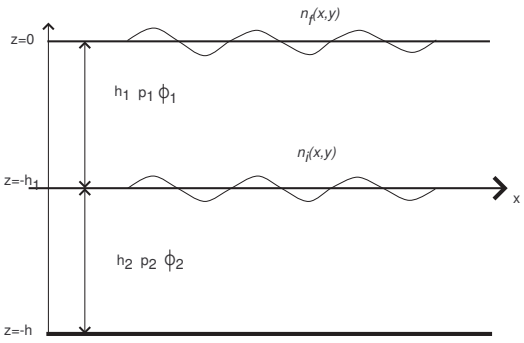

Figure-2
A definition sketch for a two-layer fluid with free surface on top

The usual assumptions of the the linearized theory and removal of the harmonic time dependant $e^{-i\omega t}$ lead to the equations for the time dependant velocity potential, $\phi(x,y,z)$

$$\phi(x,y,z) = \begin{cases} \phi_1(x,y,z,t), & -h_1 \le z \le 0, \\ \phi_2(x,y,z,t), & -h \le z \le -h_1. \end{cases} \quad (2)$$

These equations therefore can be solved by using the following conditions on all the boundaries of the domain:

$$\frac{\partial \phi_1}{\partial z} - K\phi_1 = 0, \qquad z = 0, \quad (3)$$

$$\frac{\partial \phi_1}{\partial z} = \frac{\partial \phi_2}{\partial z}, \qquad z = -h_1, \quad (4)$$

$$\rho_1\left(\frac{\partial \phi_1}{\partial z} - K\phi_1\right) = \rho_2\left(\frac{\partial \phi_2}{\partial z} - K\phi_1\right), \quad z = -h_1, \quad (5)$$

$$\frac{\partial^2 \phi_2}{\partial z^2} + \nabla h \cdot \nabla^2 \phi_2 = 0, \qquad z = -h, \quad (6)$$

$$\frac{\partial^2 \phi_2}{\partial z^2} + \nabla^2 \phi_2 = 0, \qquad -h \le z \le -h_1, \quad (7)$$

where $K = \omega^2/g$, $\nabla = (\partial/\partial x, \partial/\partial y)$, g is the gravitational acceleration, and the densities and the waves heights of the upper and lower fluid layers are denoted by ρ_1, h_1, and ρ_2, h_2 respectively, with $\rho_1 \le \rho_2$ and $h = h_1 + h_2$. Using the separation of variables, we set $\phi_j(x,y,z) = X_j(x,y)Z_j(z)$, in the equations above, where j= 1,2, and we obtained

$$\frac{\partial^2 Z_1}{\partial z^2} + k^2 Z_1 = 0, \qquad -h_1 \le z \le 0, \quad (8)$$

$$\frac{\partial Z_1}{\partial z} - KZ_1 = 0, \qquad z = 0, \quad (9)$$

$$\frac{\partial Z_1}{\partial z} = \frac{\partial Z_2}{\partial z}, \qquad z = -h_1, \quad (10)$$

$$\rho_1\left(\frac{\partial Z_1}{\partial z} - KZ_1\right) = \rho_2\left(\frac{\partial Z_2}{\partial z} - KZ_1\right), \quad z = -h_1, \quad (11)$$

$$\frac{\partial^2 Z_2}{\partial z^2} + \nabla h \cdot \nabla^2 Z_2 = 0, \qquad z = -h, \quad (12)$$

$$\frac{\partial^2 Z_2}{\partial z^2} + k^2 Z_2 = 0, \qquad -h \le z \le -h_1, \tag{13}$$

a direct solution for these equations are

$$Z_1 = k\cosh(kz) + K\sinh(kz), \quad h_1 \le z \le 0, \tag{14}$$

$$Z_2 = \frac{k\cosh(kh_1)+K\sinh(kh_1)}{\sinh(kh_2)}\cosh\big(k(z+h)\big), -h \le z \le -h_1 \tag{15}$$

with the wave number k satisfying the dispersion relation

$$\omega^4(\rho_1\,\rho_2\coth(kh_1)\coth(kh_2)) - \omega^2 gk\,\rho_2(\coth(kh_1)\coth(kh_2)) + g^2k^2(\rho_2-\rho_1) = 0 \tag{16}$$

Since equation (16) is a quadratic in ω^2, there are two possible roots of ω. These two roots correspond to each layer of the fluids, one is for the upper layer and another one is for the lower layer. Equation (16) can also be reduced to a single-layer fluid when $\rho_1 = \rho_2$[13].

The mild-slope equation in a two-layer fluid model: By assuming that the variation of water depth is moderate, the velocity potential can be written as

$$\phi_1(x,y,z) = i\,\frac{g}{w}\eta_f Z_1, \quad -h_1 \le z \le 0, \tag{17}$$

$$\phi_2(x,y,z) = i\,\frac{g}{w}\eta_i Z_2, \quad -h \le z \le -h_1, \tag{18}$$

and the relationship between η_f and η_i is given by

$$\frac{\eta_f}{\eta_i} = \frac{K}{k\sinh(kh_1) - K\cosh(kh_1)}, \tag{19}$$

with η_f and η_i are the free surface waves elevation and interfacial waves elevation, respectively. Then, η_f and η_i can be written as

$$\eta_f = a_i\exp\big(i(kx-\omega t)\big), \qquad -h_1 \le z \le 0, \tag{20}$$

$$\eta_i = b_i\exp\big(i(kx-\omega t)\big), \qquad -h \le z \le h_1, \tag{21}$$

where a_i and b_i are the incident wave amplitudes for the free and interfacial waves respectively. Considering equations (3) and (7) as an ordinary differential equation in z, and applying the integration by substitution, we have

$$\int_{-h_1}^{0}(k^2\phi_1 Z_1 + Z_1\nabla^2\phi_1)\,dz + \int_{-h_1}^{0}(k^2\phi_2 Z_2 + Z_2\nabla^2\phi_2)\,dz = -(Z_1\nabla h_1\cdot\nabla\phi_1)_{z=0} - (Z_2\nabla h_2\cdot\nabla\phi_2)_{z=-h} \tag{22}$$

By calculating $\nabla\phi_1, \nabla^2\phi_1, \nabla\phi_2$ and $\nabla^2\phi_2$ from equations (17) and (18), then substituting back into equation (22), we have obtained by neglecting the higher-order terms, the equation for the free surface waves as

$$\nabla\cdot\big(A_1\cdot\eta_f\big) + k^2A_1\eta_f + \nabla\cdot(A_2\cdot\eta_i) + k^2A_2\eta_i = 0, \tag{23}$$

where

$$A_1 = \int_{-h_1}^{0} Z_1^2\,dz \tag{24}$$

$$A_2 = \int_{-h_2}^{-h_1} Z_2^2\,dz \tag{25}$$

At the interface, by utilizing equation (21) and equations (24) and (25), and following the derivation for mild-slope equation, we have equations (23) and (26) are the mild-slope equation for the two-layer fluid model with the free surface on the top. These equations can be reduced to a single-layer mild-slope equation derived by Smith and Sprinks[14], when $\rho_1 = \rho_2$. Thus, the single-layer mild-slope equation is a special case for two-layer mild-slope equation, as we have expected.

$$\nabla\cdot(A_2\cdot\eta_i) + k^2A_2\eta_i = 0 \tag{26}$$

Wave diffraction around floating structure over a variable water depth: Consider a train of plane long waves which propagates in two-layer fluids with constant water depth h_{10} and h_{20} and is refracted by an axi-symmetric hump-shaped shoal located on the ocean floor and diffracted by a hollow cylinder located at the free surface of the upper layer as illustrated in figure 3.

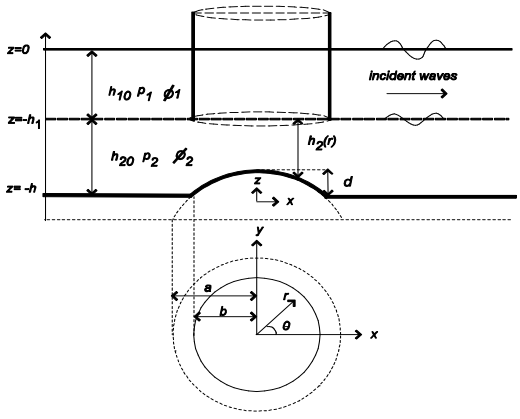

Figure-3
A definition sketch of a hump located on the floor in a two-layer fluid system

The water depth for the lower layer is prescribed by a parabolic function:

$$h_2 = \begin{cases} (h_{20}-d)\left(1+\frac{r^2}{a^2}\right), & r < b, \\ h_{20}, & r \ge b, \end{cases} \tag{27}$$

with r being the radial distance from the origin, and θ being the angle measured counterclockwise from the positive $x-$axis, b is the hump radius, d is the hump height, a and is determined by $a = b\sqrt{\frac{h_{20}-d}{d}}$ for a given set of d and h_{20} with $a > b$.

By setting $\rho_1 = \rho_2$, for the lower layer, the solution that we have here is similar to the solution given by Zhu and Harun[15] in the form of:

$$\eta_i^{out} = \sum_{n=0}^{\infty}\left(b_i i^n \in_n J_n(kr) + D_n H_n^{(1)}(kr)\right)\cos(n\theta), \tag{28}$$

$$\eta_i^{in} = \sum_{n=0}^{\infty} B_n R_n(r)\cos(n\theta), \tag{29}$$

where

$$R_n(r) = \sum_{n=0}^{\infty} \alpha_{m.n} r^{m+n}$$

$$B_n = b_i k\, i^n \in_n \frac{J_n(kb)H_n^{(1)}(kb) - J_n'(kb)H_n^{(1)}(kb)}{kR_n(b)H_n^{(1)}(kb) - R_n'(b)H_n^{(1)}(kb)}, \quad (30)$$

$$D_n = b_i\, i^n \in_n \frac{kJ'_n(kb)R_n(b) - J_n(kb)R_n'(b)}{R'_n(b)H_n^{(1)}(kb) - kR_n(b)H_n^{'(1)}(kb)},$$

and the solution for $\alpha_{m,n}$ is obtained by using the Frobenius series solution and is in the form of

$$\alpha_{0,n} = 1, \quad (31)$$

$$\alpha_{1,n} = 0,$$

$$\alpha_{m+2,n} = -\frac{(m+n)(m+n+2)+v^2-n^2}{a^2(m+2)(m+2n+2)}\alpha_{m,n}, \quad (32)$$

$$m = 0,1,2, \ldots$$

For the upper layer, inside the cylinder, we have the solution in the form of:

$$R_{1,n}^{in} = C_{9,n}J_n(kr) - Y_n(kr)\int_0^r \frac{\pi r B_n R_n(r) J_n(kr)}{2} dr + J_n(kr)\int_0^r \frac{\pi r B_n R_n(r) Y_n(kr)}{2} dr \quad (33)$$

where

$$C_{9,n} = \frac{Y_n'(kb)}{J_n'(kb)}\int_0^r \frac{\pi r\, B_n R_n(r) J_n(kr)}{2} dr - \int_0^r \frac{\pi r\, B_n R_n(r) Y_n(kr)}{2} dr \quad (34)$$

For the region outside the cylinder in the upper layer, we have

$$R_{in}^{out} = D_{1,n}J_n(kr) + D_{2,n}H_n(kr) - H_n(kr)\int_0^r \frac{i\pi r\, D_n H_n(kr) J_n(kr)}{2} dr + J_n(kr)\int_0^r \frac{i\pi r\, D_n H_n(kr) H_n(kr)}{2} dr \quad (35)$$

where

$$D_{1,n} = -\int_b^{\infty} \frac{i\pi r\, D_n H_n(kr) H_n(kr)}{2} dr \quad (36)$$

$$D_{2,n} = -\left(a_i i^n \in_n + D_{1,n}\right)\frac{J_n'(kr)}{H_n'(kr)} \quad (37)$$

If we set $h_{20} = 0$, for $d \geq 0$, in equation (37), we found that the inhomogeneous terms in this equation and the lower layer equation are vanished, resulting in only the Hemholtz equation. As a result, equation (37) also reduces to Mac Camy and Fuchs[11] solution. Thus, the Mac Camy and Fuchs[11] solution is a special case for our solution when $h_{20} = 0$, as we have expected.

Results and Discussion

Comparison with the Mac Camy and Fuchs Solutions: Since the mild-slope equation for a two-layer fluid model should be reduced to the Hemholtz Equations model when $h_{20} = 0$, it would be interesting to compare both models, as part of the verification process.

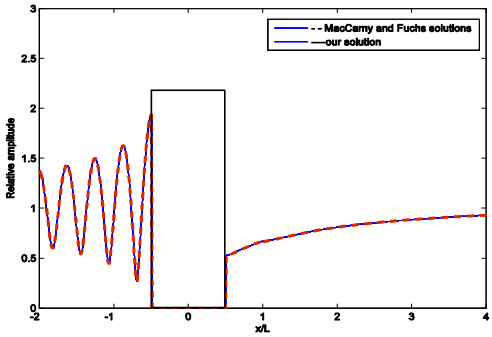

Figure-4
Comparison of relative wave amplitudes between MacCamy and Fuchs solution and our solution when $h_{20} = 0$ along *x*-axis

We set $h_{10} = 2.4$ and $h_{20} = 0$, and take the remaining parameters exactly the same as those used in single-layer fluid model discussed in Zhu and Harun[15], i.e, $b/L = 0.5$, and the wave length, $L = 120.4$. Since, the analytic solution for η involves an infinite series, it must be truncated for the purpose of numerical solution, so we set $N = 70$ and $M = 30$, because the solution had already converged with these values. The Bessel and Hankel functions in the analytical solution were computed using the built-in subroutines in MATLAB.

Figure 4 shows the comparison of the relative wave amplitudes along the *x*- axis for the two and single-layer fluid models. The results in this comparison are presented in terms of dimensionless coordinates, *x/L* and the center of the hump is located at the origin. As expected, both solutions are identical and hardly distinguishable. With the excellent agreement between these solutions, we are confident that the derivation of our new analytical solution is correct.

Comparison with the flat bottom: As we already know, the flat bottom is the special case for the variable water depth with hump is located on the sea floor. Therefore, to gain confidence for the non-flat-bottom solution, and in order to further verify the newly derived equation, we have compared the solution that we obtained from the flat bottom with the solution with a very small size hump, $d = 10^{-6}$ being placed on the seabed.

The comparison for these two problems is shown in Figure 5. As can been seen, both figures are identical and can't be distinguished. Therefore, this adds to our confidence that our derivation was derived correctly. In addition, for the flat bottom case, we discovered that it seemed like there was a plane wave propagating inside the cylinder because based on our derivation, the lower layer is presented by the plane waves.

Topographic and radius Effects: In this section, we discuss the effects of the wave refraction when the hump height and

radius of the cylinder are varied, while other parameters are held constant.

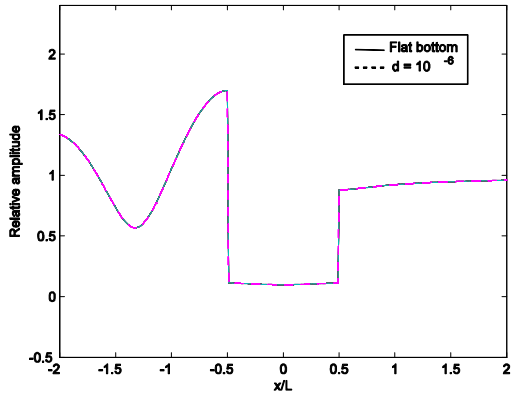

Figure-5
Comparison of relative wave amplitudes between the flat sea bottom and tiny little hump along the *x*-axis

In Figure 6, we plot the relative wave amplitudes along the $y-$axis for different cylinder radii, b/L = 0.25, 0.5, and 1.0 with a fixed d = 0.25 and $h_{10} = h_{20}$ = 4.8, respectively.

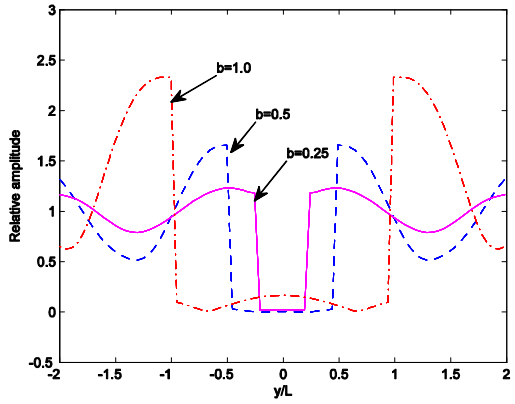

Figure-6
Comparison of relative wave amplitudes along the *y*axis with *b/L* varied

As the radius of the hump, b/L is increased, the relative wave amplitude inside and outside the cylinder also increased as can be seen along the y- axis. This is due to the concentration of wave energy in the lee region of an obstacle, as a result of refractive and diffractive focusing, when the disturbance of the obstacle is sufficiently large. However, for a small hump radius no waves are found inside the cylinder because the latter is smaller than the wavelength, as can be clearly seen in figure 6.

Next, we discuss the effects of the wave refraction when the height of the hump, d is varied. Figure 7 show the relative wave amplitude along the $x-$ axis, for the cases of d = 0.05, 0.25, and 0.5 with the hump radius being fixed at b/L = 0.5, and $h_{10} = h_{20}$ = 4.8. As can be clearly seen from figure 7, as the height of the hump increases, the relative wave amplitude becomes larger as expected.

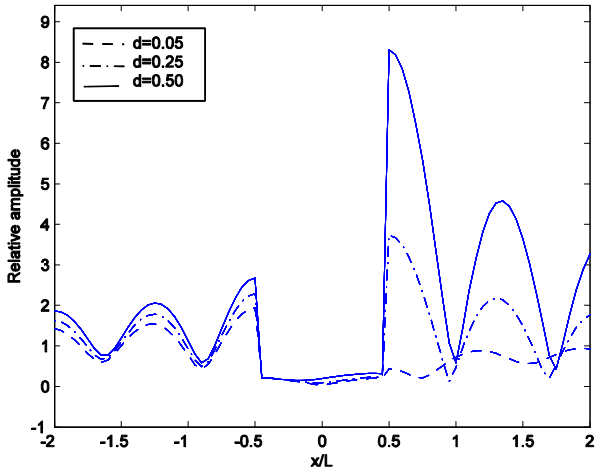

Figure-7
Comparison of relative wave amplitudes along the *x*-axis with *d* varied

For a hump with a smaller hump height, d, the refraction effects are weak, resulting in smaller wave heights inside and outside the cylinder. On the other hand, for a higher hump height, d, there is more refractive focusing and thus the reaction to the disturbances behind the hump is larger in comparison with the lower d. For example, along the $x-$axis, as we increase the height of the hump, from 0.05 to 0.25, the maximum value of relative wave amplitude outside the cylinder obtained has increased too from 0.5 to 4.1, and if we further increase the hump height to 0.5, the maximum value of relative wave amplitude obtained is about 8.5. Therefore, we can conclude that, the higher the hump high is, the bigger is relative waves amplitude will observed. Hence, the OWC device should be installed in the shallow water, where waves would produce more energy through the diffraction, refraction and shoaling processes.

Effect of the cylinder height: In this section, we discuss the effect of the wave refraction when the height of the cylinder, h_{10}, is varied, while other parameters are held constant. To examine this, we set h_{10} = 2.4, 4.8, and 7.2 with the hump radius being fixed at b/L = 0.5, d/L = 0.5 and h_{20} = 4.8.

The comparison for each value of h_{10} along the x- axis is shown in figure 8. It can be obviously seen that, an increase in the height of the cylinder, h_{10}, results in larger relative wave amplitudes. From the figure, when we set h_{10} = 2.4, half of the reference cylinder height, h_{10} = 4.8, we can see that, the relative wave amplitude was decreasing with the decrease of the cylinder height. On the other hand, when the height of the cylinder is 1/2 times higher than the reference cylinder, the relative amplitude also becomes bigger in the disturbance area. This shows that, the refractive and diffractive effects become stronger when we place a bigger obstacle in front of the waves, resulting in bigger relative amplitude in the lee region.

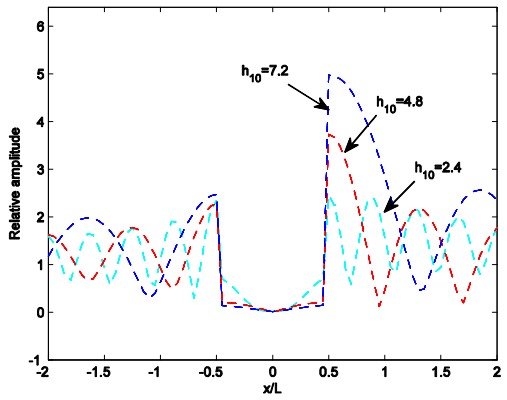

Figure-8
Comparison of relative wave amplitudes when h_{10} are varied along the x-axis

Conclusion

The long waves propagating in single-layer fluid over a circular hump with hollow cylinder located at the free surface by using the mild-slope equation in two-layer fluid model with free surface on the top is studied in this paper. We also compared our solution with MacCamy and Fuchs solution when our solutions were reduced to their case when $h_{20} = 0$, as part of the verification process. The two solutions were identical and hardly distinguishable. To further verify our solution, we have also compared the solution for the flat bottom and the solution with very small hump size. Once again, both solutions were identical.

Furthermore, we have also examined and discussed the effects of the height of the cylinder, hump dimensions and cylinder radius to the wave refraction and diffraction when they are varied. When there is an increase in the obstacle, the diffraction and refraction effects become stronger, resulting in a bigger relative amplitudes. This is important for OWC industry because from this results, we can find the best place to install the OWC device.

References

1. Sharmila N., Jalihal P., Swamy A.K. and Ravindran M.. Wave powered desalination system, *Energy*, **29,** 1659–1672, **(2004)**

2. Garret C.J.R., Bottomless harbor, *Journal of Fluid Mechanics*, **43(3)**, 433–449, **(1970)**

3. Evans D.V., The oscillating water column wave energy device, *J. Inst.Math. Appl*, **22**, 423–433 **(1978)**

4. Evans D.V., Wave-power absorption by sytems of oscillating surface pressure distributions, *Journal of Fluid Mechanics*, **114**, 481–99, **(1982)**

5. Smith C.M.. *Some problems in linear water waves,* PhD thesis, University of Bristol, (**1983)**

6. Sarmento A.J.N.A and Falce*a*o A.F De O.. Wave generation by an oscillating surface-pressure and its application in wave-energy extraction, *Journal of Fluid Mechanics*, **150**, 467–485, **(1985)**

7. Falce*a*o A.F. de O. and Rodrigues R.J.A., Stocastic modelling of OWC wave power plant performance. *Applied Ocean Research*, **24,** 59–71, **(2002)**

8. Falce*a*o A.F. de O.. Control of an oscillating-water-column wave power plant for maximum energy production, *Applied Ocean Research*, **24**, 73–82, **(2002)**

9. Martin-rivas H. and Mei C.C., Wave power extraction from an oscillating water column at the tip of a break water, *Journal of Fluid mechanics***, 626**, 395–414, **(2009)**

10. Martin-rivas H. and Mei C.C., Wave power extraction from an oscillating water column along a straight coast, *Ocean Engineering,* **36**, 429–433 **(2009)**

11. MacCamy R.C. and Fuchs R.A.,. Wave forces on piles: A diffraction theory, *US Army Corps of Engineering, Beach erosion Board, Washington DC, Technical Memorandum*, **69**, **(1954)**

12. Zhu S.-P. and Harun F.N., Refraction of interfacial waves by a circular hump, *Journal of Engineering and Computational Mechanics,* **162,(4),** 199-213, **(2009)**

13. Lamb H., *Hydrodynamics*. Cambridge : Cambridge University Press, sixth edition, **(1993)**

14. Smith R. and Sprinks T., Scattering of surface waves by a conical island, *J. Fluid Mech.*, **72**, 373–384 **(1975)**

15. Zhu S.-P. and Harun F.N., An analytical solution for long wave refraction over a circular hump, *J. Appl. Maths. and Comput*, **30**, 315–333 **(2009)**